IEEE Access
Multidisciplinary ⋮ Rapid Review ⋮ Open Access Journal

Received 8 September 2023, accepted 10 October 2023, date of publication 16 October 2023, date of current version 20 October 2023.

Digital Object Identifier 10.1109/ACCESS.2023.3325198

RESEARCH ARTICLE

Emergency Power Supply System for Critical Infrastructures: Design and Large Scale Hardware Demonstration

SOHAM CHAKRABORTY[1], (Member, IEEE), JAESANG PARK[2], (Graduate Student Member, IEEE), GOVIND SARASWAT[2], (Senior Member, IEEE), TOBY MEYERS[2], (Member, IEEE), JING WANG[2], (Senior Member, IEEE), SOUMYA TIWARI[2], (Member, IEEE), VIVEK KHATANA[1], (Graduate Student Member, IEEE), ATIF MAQSOOD[3], APURVA SOMANI[3], AND MURTI V. SALAPAKA[1], (Fellow, IEEE)

[1]Department of Electrical and Computer Engineering,University of Minnesota, Minneapolis, MN 55455, USA
[2]National Renewable Energy Laboratory, Golden, CO 80401, USA
[3]Dynapower Company LLC, South Burlington, VT 05403, USA

Corresponding author: Soham Chakraborty (chakr138@umn.edu)

This work was supported in part by the Advanced Research Projects Agency-Energy (ARPA-E) through the project titled ''Rapidly Viable Sustained Grid'' under Grant DE-AR0001016; and in part by the National Renewable Energy Laboratory, operated by Alliance for Sustainable Energy, LLC, for the U.S. Department of Energy (DOE) under Contract DE-AC36-08GO28308.

ABSTRACT Seamless recovery and sustained power to critical infrastructures (CIs), after grid failure, is a crucial need arising in disaster scenarios that are increasingly becoming more frequent. Accreditation standards recommend CIs to have emergency power supply system (EPSS) in order to form a local microgrid network with backup resources (generation units/renewable resources) in case of sudden power blackouts of main grid supply. The standards also recommend enhancements such as seamless transition capability during on-grid to off-grid jump and vice versa, efficient and optimal operation while maintaining the standard regulation and power quality limits during power contingencies, and operation with sustenance of reliable power for long periods of time. This article is proposing a comprehensive design of the EPSS for uninterrupted operation of CIs by employing novel techniques, such as 1) mode-dependent droop controlled grid-forming inverters for seamless transition capability; 2) fast-acting optimal net-load management engine for efficient and optimal operations maintaining regulation and power quality limits; 3) optimization-based horizon of viability engine for longer, sustained and viable operation in the aftermath of grid failure as recommended in standards. Two stage validations are conducted using defined test cases while considering various types of contingencies on a 3-ϕ, 60 Hz, 480 V, 450 kVA test system based on a realistic electrical network of a commercial scale medical center. The comprehensive controller-hardware-in-loop and power-hardware-in-the-loop based experiments corroborate the efficacy and robustness of the proposed strategy for EPSS employed in the CI. The mode-dependent droop controller enables seamless transition of the critical infrastructure between the off-grid and the on-grid modes. Inverters operate in the gird-forming mode when the CI is off-grid and also when the CI is on-grid while keeping frequency and voltage regulated between ± 0.5 Hz and $\pm 10\%$ of the nominal respectively. The fast-acting net-load management engine maintains the balance in total available generation and the power demand by determining the optimal decisions within 100 ms during various contingencies while regulating the voltage, frequency, and total harmonic distortion (THD) of the system under the strict limit recommended by the grid codes. The horizon of viability optimization engine showcases advantages over conventional scheduling engines with higher utilization of critical loads and maintaining higher energy at the end of an 1-hour experiment.

The associate editor coordinating the review of this manuscript and approving it for publication was Ehab Elsayed Elattar.

INDEX TERMS Droop control, emergency power supply system, generation scheduling, load management, parallel inverters.

I. INTRODUCTION

Critical infrastructure (CI) describe essential assets of society, including medical centers, security service centers, food production and distribution centers, and communication facilities. Disruption of power to CI often results in a debilitating impacts on physical and economic security as well as public health and safety. The rapid recovery of power, possibly after a power blackout caused by increasingly frequent weather/climate disasters, for CI is a crucial need [1].

Accreditation standards, such as IEEE 602, require CI to have an emergency power supply system (EPSS) to form a local microgrid network with local generation and automatic transfer switches, in case of sudden power blackouts of the main grid supply [2]. Depending on the level of criticality and the urgency of the electrical loads, the EPSS is required to form the local microgrid within a specified amount of time to restore the operation of the CI. Various types of EPSS include Type-U characterizing uninterruptible EPSS, and Type-10 where the EPSS is allowed 10 s for recovery [3], [4]). Gas/diesel generator sets are traditional choices for most CI as local energy units for EPSS due to their sustained and robust power supply capability; however, the long startup time from standby mode makes the task of a seamless and rapid power restoration of CI difficult to achieve with these sources [5]. Battery energy storage units interfaced with power electronic inverters provide uninterrupted power supply (UPS) system that are an alternate solution that enhances the ease in operation and reduces the response time of EPSS for CI. Accreditation standards, such as NFPA 111, recommend stored-energy EPSS (SEPSS), which employ batteries/fuelcells/ultracapacitors as the main energy harvesting units along with inverter topology to assist in restoring of power to CI in the case of the grid failure [6]. Briefly, these standards for CI recommend the following:

- To circumvent any short/temporary electrical interruptions to the critical and sensitive loads of the CI, Type-O/Type-U SEPSS are recommended, which posses the capability of seamless transition during the on-grid to off-grid jump and vice versa.
- The EPSS is recommended to efficiently operate the CI, by maintaining standard regulation and power quality limits and to operate optimally enabling smart and dynamic prioritizing of critical loads based on real-time situational awareness of the overall system.
- After the initial recovery from a power blackout, the EPSS is recommended to operate the CI while sustaining reliable power for long periods of time in such emergency situations.

In [7], a comprehensive literature review is conducted on service restoration through microgrid formation techniques for distribution networks. Planning and service restoration through microgrid formation, virtual power plants, grid-forming inverters and smart circuit breakers are some promising solutions for emergency power systems [8], [9], [10]. However, a thorough design and procedure for restoration of a microgrid network after power blackout are not discussed in these works. Moreover, being compliant with the grid regulation code during the restoration process is critical for the health of equipment in critical infrastructures. The role of power electronic converters in climate emergency is highlighted in [11]. References [12], [13], [14], [15], and [16] develop emergency power systems that address prolonged power blackouts for various facilities such as hybrid advanced traction power supply system and medical centers. To the best of the authors' knowledge, there are no works present in the current literature that provide a comprehensive framework/strategy for EPSS to operate CI with the recommendations of NFPA 111 under emergency situations [17], [18], [19], [20]. This article proposes a comprehensive design of an EPSS for the uninterrupted operation of CI by employing novel techniques to enhance the capabilities of the EPSS as recommended in the standards.

1) The seamless transition capability of the EPSS is achieved by using novel mode-dependent droop-controlled grid-forming (GFM) inverters [21]. The control strategy achieves the following objectives: 1) the seamless transition and recovery of power by the GFM inverters after the grid failure and 2) the seamless transition and re-synchronization by the GFM inverters after the grid returns. Further, the control strategy only requires information on the grid switch status for the mode transition. The advantage of the seamless transition capability, as proposed in [21], is that it does not require an additional control layer and parameter tuning to restore the voltage, frequency, and phase during transitions and synchronizations. Moreover, it ensures significantly less deviations in the output voltage/current of the inverters during the switching of its operating mode, unlike some existing works [22], [23], [24], [25]. The seamless control strategy of [21] is selected as a good candidate for this EPSS application.
2) To enhance the quality, resiliency, and reliability of the EPSS in the operation of the CI, this article proposes a centralized, high-speed, and cost-optimal coordination and allocation of loads during operational contingencies as an essential improvement, especially during off-grid mode of operation after the grid failure or during a complete black start operation of the CI [26], [27]. Unlike some existing works [28], [29], the ''net-load management'' (NLM) engine of [26], [27] is superior in the optimal coordination process in applications with much larger numbers of net-load resources and fast-changing generation resources. It is

also capable of accurately meeting a specific aggregate power set point to generation resources while achieving dispatch on a faster timescale and maintaining the standard regulation and power quality limits.

3) To guarantee the viability of a sustained, reliable supply of power over a substantial time horizon for the CI operation in the aftermath of the grid failure, an intelligent optimization scheme, the "horizon of viability" (HoV) engine, based on the cost-optimal portfolio of the locally available distributed energy resources (DERs) and the loads, is proposed and employed in the EPSS [30]. The advantage of the proposed HoV engine over existing works [31], [32], [33], [34], is that it ensures sustained viable operation of the CI for a longer time horizon by supplying critical, sub-critical, and non-critical loads via using the backup DERs based on the historical load and solar irradiance forecast profiles and the real-time awareness of the run-time capabilities of the DERs.

This article assimilates three novel techniques for enhancing the capability of the EPSS of CI. These are as follows:

1) mode-dependent integrator-based droop-controlled grid forming inverters for seamless transition capability of the EPSS during on-grid to off-grid jump and vice versa [21],
2) fast-acting optimal net-load management engine for efficient and optimal operations of the EPSS, maintaining regulation and power quality limits throughout the operation [26],
3) optimization-based horizon of viability engine for longer, sustained and viable operation of the EPSS via local and emergency energy resources in the aftermath of grid failure [30].

The main challenge here, is to employ all three techniques and operate all of these simultaneously so that the combined functionalities of these novel techniques serve the purpose of enhancing the capability of the EPSS of the CI. Therefore, the main contribution of this article is to provide a systematic guidelines for implementing such novel techniques for EPSS of the CI and highlighting the key challenges in the implementation and operation of such large system. The proposed advancements for EPSS of a CI are validated in two stages using defined test cases while considering various contingencies. In the first stage, a controller hardware-in-the-loop (CHIL)-based real-time simulation study is conducted on a test system based on the realistic electrical network of a commercial-scale medical center. This stage of validation establishes the preliminary evidences showcasing the advantages of these novel techniques in the EPSS of a CI. In the second stage, a comprehensive power hardware-in-the-loop (PHIL)-based real-time study is conducted on the same electrical network. The test system under study is an R-L network of 3-ϕ, 60Hz, 480V and it has critical loads of 150kW, 72kVAr; sub-critical loads of 60kW, 30kVAr; and non-critical loads of 240kW, 115kVAr. The test system is

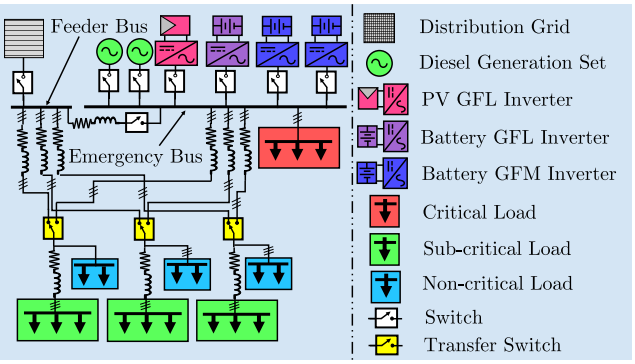

FIGURE 1. The power circuit of the critical infrastructure under study.

equipped with two 3-ϕ, 125-kVA, 4-quadrant GFM inverters, two 3-ϕ, 125-kVA, 4-quadrant GFL inverters, and, one 3-ϕ, 135-kW diesel genset. The large-scale PHIL-based validation corroborates the fact that the employment of these novel techniques enhances the capabilities of the EPSS of a CI.

This article is organized as follows. Section II presents the description of the existing EPSS of a CI. Section III highlights the proposed enhancements for the EPSS of the CI, and Section IV describes the enhancements in detail. Section V focuses on the test cases to be used for the validation. Section VI and Section VII show the CHIL and PHIL experimental setup and the corresponding results, respectively. A summarized discussion on the hardware results are provided in Section VIII. Finally, Section IX concludes the article.

II. DESCRIPTION OF THE EXISTING EPSS OF THE CI

A. EXISTING POWER CIRCUIT AND OPERATIONAL ENGINE OF THE CI

The one-line diagram of the 3-ϕ power circuit of the CI is shown in Fig. 1. The considered CI has three classifications of loads, as defined in NFPA 99 [3], namely: i) critical load: loads that need continuous uninterrupted power supply irrespective of the grid availability (e.g., critical operation room, life-saving equipment in a medical center); ii) sub-critical load: loads that allow the temporary shutdown of services in case of grid failures (e.g., general patient room, HVAC system in a medical center); and iii) non-critical load: loads that allows temporary/permanent shutdown of services in case of grid failures (e.g., public lighting and elevators in a medical center). The building electrical network of the CI has a main feeder bus and an emergency bus and are connected to each other via a switch. Loads are connected to the buses via transfer switches. The grid is connected to the feeder bus via a feeder switch. At the emergency bus, multiple emergency DERs are connected via switches in parallel. They include two diesel generation sets, two GFM battery inverter systems, one solar inverter system, and one grid-following (GFL) mobile battery inverter system. The diesel generation sets are operated with load-frequency-based governor control and voltage-reactive power-based

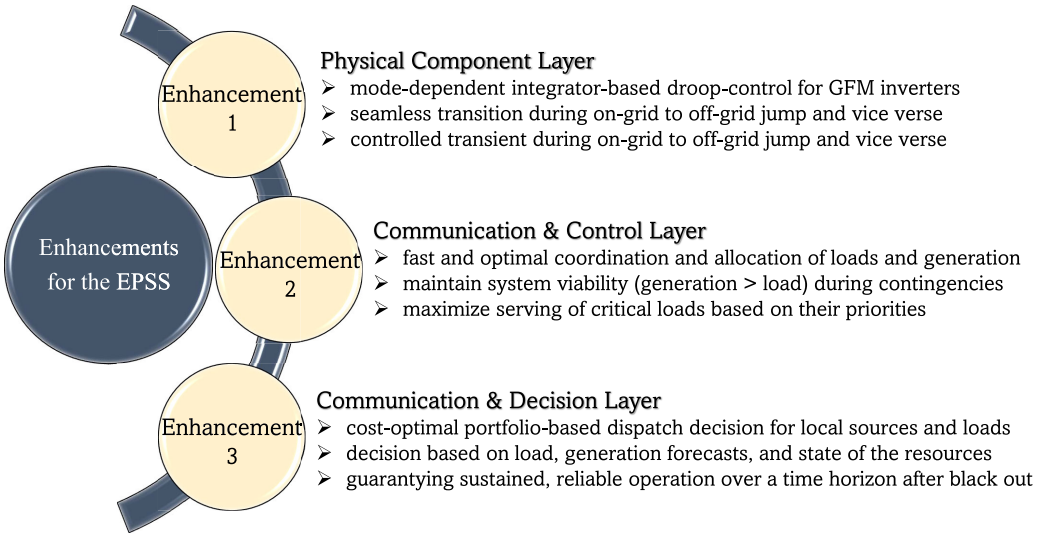

FIGURE 2. The methodology flowchart of the proposed enhancements for the emergency power supply system of a critical infrastructure.

automatic voltage regulator control [35]. The solar and mobile battery inverter system are operated in GFL mode with a d-q axis-based conventional inner-current controller and globally/locally provided P-Q set points [36]. The battery inverter systems are operated in conventional GFM mode with d-q axis-based conventional outer-voltage-inner-current controller and P-f/Q-V-based droop control laws [37]. The existing EPSS of the CI enables the following:

- In on-grid mode, the grid at the feeder bus is the main power supply of the CI. At the emergency bus, apart from the solar GFL inverter, all other DERs are disconnected. While the main grid is available, the total demand of the CI (i.e., entire critical, sub-critical, and non-critical loads) is met. The EPSS enables the entire sets of load to be activated due to the availability of the grid.
- In off-grid mode, the DERs in the emergency bus are the main power supply of the CI. In case of a grid failure, the EPSS activates its emergency protocol for operation, and the operational engine starts priority-based load shedding, which is decided by the criticality of the loads. As a result, the EPSS supplies only the critical loads for sustained and viable emergency operation depending on the available rating of the DERs.

B. CHALLENGES IN THE EXISTING EPSS FOR CI

The existing EPSS for CI has the following challenges:

- The existing EPSS is unable to provide a rapid and seamless power recovery (on-grid to off-grid transition and vice versa without electrical interruption) in case of a grid failure. The fundamental cause is the types of DERs and their control architectures. For example, traditional gas/diesel generator sets, while having sustained and robust power supply capability, have inherently long startup times from standby mode [4]. The GFM battery inverter system (not connected to the emergency bus during on-grid mode), while having a quick startup time, can supply power only after successful synchronization and connection of the switches to the emergency buses [6]; therefore, with the existing EPSS management for the CI, Type-U-based emergency recovery (seamless power restoration) of the entire CI is challenging.
- The existing EPSS load management engine is not designed for the sustained and viable operation of the CI in emergency situations. Currently, the operational engine follows a mere brute-force method to allocate loads based on their criticality for CI operation, depending on the available DER capability. As a result, it cannot operate the CI optimally (in the sense of the allocation of critical loads and longer viable operation of CI) during emergency situations. A centralized and intelligent control and monitoring method of the system, including sources and loads, to obtain the situational awareness and to take automatic corrective actions is lacking.

III. PROPOSED ENHANCEMENTS OF THE EPSS FOR CI

To overcome the challenges mentioned in Section II-B, this article proposes various enhancements to be employed in the EPSS for the CI. The proposed enhancements in the EPSS aims to achieve (i) seamless transitions of the CI from on-grid to off-grid transition and vice versa, (ii) centralized load management control to optimally manage the CI operation, (iii) intelligent load management for longer viable operation during emergency situations. The methodology flowchart of the proposed enhancements for EPSS of a CI is shown in Figure 2. The proposed enhancements are further described as follows:

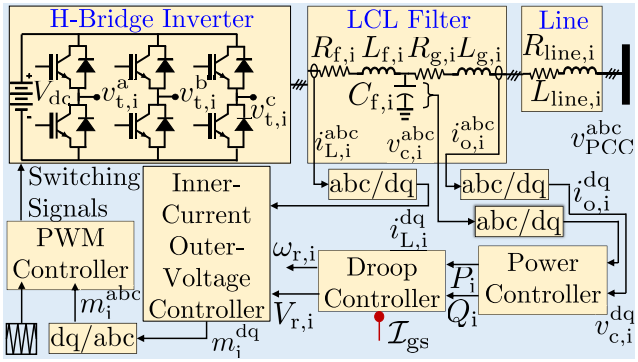

FIGURE 3. The power circuit and various control loops for the i^{th} GFM inverter.

- **Enhancement 1**: Ensuring seamless transitions (i.e., without any electrical interruption to the loads of the CI) from on-grid to off-grid and from off-grid to on-grid is an essential improvement for the uninterrupted operation and health of sensitive loads of the CI during emergency situations. As mentioned in Section II-B, the existing circuitry and control architectures of the DERs are unable to provide seamless transition capability. The modification in the droop control law of the GFM battery inverters, as mentioned in Section IV-A, is proposed to achieve seamless transition capability [21].
- **Enhancement 2**: Ensuring fast and optimal coordination and allocation of loads during operational contingencies in the CI based on its criticality is another essential improvement for the EPSS, especially during off-grid mode of operation after the grid failure or during a complete black-start operation of the CI. The employment of the proposed centralized NLM engine, as mentioned in Section IV-B, ensures enhancing the quality, resiliency, and reliability of the emergency power supply operation of the CI [26], [27].
- **Enhancement 3**: Guarantying the viability of a sustained, reliable supply of power over a substantial time horizon is crucial for CI operation in the aftermath of a grid failure caused by increasingly frequent catastrophic events. An intelligent optimization scheme based on the cost-optimal portfolio of the locally available DERs and the loads, leveraged by the increasing expertise in accurate load and generation forecasts, is employed in the EPSS of the CI to achieve the target [30], as mentioned in Section IV-C.

IV. DESCRIPTION OF THE PROPOSED MODIFICATIONS

A. MODIFIED DROOP LAW FOR SEAMLESS TRANSITION CAPABILITY

The proposed control strategy of the inverters aims to achieve the following objectives: 1) regulate the output active and reactive power by the droop-based battery inverters to a desired value while operating in on-grid mode, 2) perform seamless transition and recovery of power injections into the critical loads after a grid failure by the inverters operating in GFM mode all the time, 3) require minimal, single-bit information on the grid status for the mode transition of droop control. The design guidelines and the control architecture are briefly described below. Reader can find detailed descriptions in reference [21]. The power circuit of the i^{th}, 3-ϕ H-bridge inverter is shown in Fig. 3. It is connected to the network at point-of-common-coupling via an LCL filter and a coupling line. The control architecture, as shown in Fig. 4, is described here.

1) POWER CONTROLLER

It determines the averaged active, P_{i}, and reactive power, Q_{i}, of the i^{th} GFM inverter as follows:

$$P_{\text{i}} = \frac{1}{\tau_{\text{S,i}}s + 1} p_{\text{i}}, \tag{1}$$

$$Q_{\text{i}} = \frac{1}{\tau_{\text{S,i}}s + 1} q_{\text{i}}, \tag{2}$$

where,

$$p_{\text{i}} := \frac{2}{3}[v^{\text{d}}_{\text{o,i}} i^{\text{d}}_{\text{o,i}} + v^{\text{q}}_{\text{o,i}} i^{\text{q}}_{\text{o,i}}], \tag{3}$$

$$q_{\text{i}} := \frac{2}{3}[v^{\text{q}}_{\text{o,i}} i^{\text{d}}_{\text{o,i}} - v^{\text{d}}_{\text{o,i}} i^{\text{q}}_{\text{o,i}}], \tag{4}$$

where, $v^{\text{d}}_{\text{o,i}}$, $v^{\text{d}}_{\text{o,i}}$, $i^{\text{d}}_{\text{o,i}}$, $i^{\text{q}}_{\text{o,i}}$ are the dq-components of output voltage and current and $\tau_{\text{S,i}} \in \mathbb{R}_{>0}$ is the time constant of the low-pass filters.

2) DROOP CONTROLLER

The mode-dependent droop controller for the GFM inverter for both the on-grid and off-grid operation of the CI is shown in Fig. 4. The proposed droop law is as follows:

$$\omega_{\text{r,i}} = \omega_{\text{N}} - n_{\text{i}} P_{\text{i}}, \tag{5}$$

$$V_{\text{r,i}} = V_{\text{N}} - m_{\text{i}} Q_{\text{i}} - \mathcal{I}_{\text{gs}} k_{\text{i}} \int Q_{\text{i}} \text{d}t, \tag{6}$$

where, ω_{nom}, V_{nom} are the nominal frequency (in rad/s) and voltage set-point (in volt) of the system, respectively; n_{i}, m_{i} are the coefficients of the P-f and Q-V droop law, k_{i} is the integral coefficient of the Q-V droop law. $\mathcal{I}_{\text{gs}} = 1$ and $\mathcal{I}_{\text{gs}} = 0$ in on-grid and off-grid mode respectively. $\mathcal{I}_{\text{gs}}$ ensures that the integral action in the Q-V droop is effective only in on-grid mode. This droop law ensures that the GFM inverters in on-grid mode supply no reactive power in steady state. The addition of dependency on the variable, $\mathcal{I}_{\text{gs}}$, facilitates the GFM inverters seamless functionality for CI during the transition of on-grid to off-grid and off-grid to on-grid modes. The values of n_{i} and m_{i} are typically chosen such that $\omega_{\text{r,i}}$ and $V_{\text{r,i}}$ are within the allowed specification, defined by IEEE 1547 Standard [38], for all $P_{\text{i}} \in [0, P_{\text{rated,i}}]$ and $Q_{\text{i}} \in [-Q_{\text{rated,i}}, Q_{\text{rated,i}}]$ respectively. Here, $P_{\text{rated,i}}$ and $Q_{\text{rated,i}}$ are the rated active and reactive powers that can be delivered by the i$^{\text{th}}$ GFM inverter. The saturation limit in the integrator of the Q-V droop law ensures that the

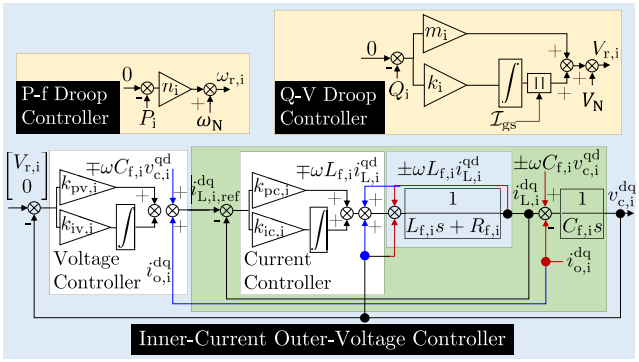

FIGURE 4. Inner-current-outer-voltage control loop with the proposed modified P-f, Q-V droop controller for the i^{th} GFM inverter.

entire system remains viable under compromised scenarios including significant delay in communicating $\mathcal{I}_{\text{gs}}$ which results in undesirable active integral operation during off-grid mode. A good candidate for selecting the magnitude of the upper and lower saturation limit of the integrator, $\pm\Delta V$, is $\pm 10\%$ of the nominal voltage rating as recommended by limits of IEEE 446 [5].

3) INNER-CURRENT-OUTER-VOLTAGE CONTROLLER

The conventional inner-current-outer-voltage controller is employed here, as shown in Fig. 4. For the inner-current controller, a proportional-integral (PI) compensator with parameters $k_{\text{pc,i}}$ and $k_{\text{ic,i}}$, is used for tracking the reference of the dq-axis inductor current with the desired time constant, $\tau_{\text{c,i}}$ (typical range from $0.5-2$ ms) [39]. Similarly, for the outer-voltage controller, a PI compensator, with parameters $k_{\text{pv,i}}$ and $k_{\text{iv,i}}$, is used to enable reference tracking with the desired phase margin and gain crossover frequency, based on the *symmetrical optimum* method [39]. Additional feed-forward signals facilitate the disturbance rejection capability of each layers.

B. NLM ENGINE FOR RELIABLE OPERATION

The NLM engine is a central dispatch control system that provides high-speed, cost-optimal coordination of a set of net loads (a combination of generation and controllable loads). The reader can find a more detailed description of the NLM engine in references [26], [27]. The high-level objectives of the NLM engine are to:

1) Maintain system viability (generation capacity > load), including a specified generation reserve margin, by triggering dispatch actions each time the generation reserve margin falls below or exceeds the target range.
2) Minimize the overall cost (the sum of the unit cost change in the active power of the net load resource for all resources) of each dispatch action.
3) Maximize the amount of controllable load that is served using the available generation based on their priorities.

The system, called as the net-load-unit (NLU), contains an aggregated single uncontrollable (critical) load; N_{d} number of controllable (non-critical) loads; N_{G} number of solar and mobile battery-based GFL battery inverter system(s) and an aggregated single entity called the *slack bus* that comprises single/multiple GFM battery inverter systems and diesel generation sets. To meet these objectives, the NLM engine at any time instant, t_0, performs the following functionalities:

1) The NLM engine receives measurements from the off-grid NLU and tracks the latest system state.
2) At each measurement update, the NLM engine evaluates the current power system operating margin (a comparison between the current operating power of the *slack bus*, $P_{\text{slk}}(t_0)$, and the largest *slack bus* capacity that can be provided, $|P_{\text{slk}}^{\max}|$) and determines if a dispatch is needed to maintain:

$$|P_{\text{slk}}^{\max}| - 2R_{\text{m}} \le P_{\text{slk}}(t_0) \le |P_{\text{slk}}^{\max}| - R_{\text{m}}, \tag{7}$$

where R_{m} is the specified reserve margin. Specifically, if $P_{\text{slk}}(t_0) > |P_{\text{slk}}^{\max}| - R_{\text{m}}$, then it commands a decrease of $P_{\text{slk}}(t_0)$. If $P_{\text{slk}}(t_0) \le |P_{\text{slk}}^{\max}| - 2R_{\text{m}}$, then it commands an increase in $P_{\text{slk}}(t_0)$.
3) If a set point is required to maintain the viability of the NLU with the margin (7), the NLM engine finds the optimal set of dispatch commands (on/off decisions for the controllable loads, dispatch set points to GFL inverters) that accomplishes these objectives using an optimization problem.

The optimization problem is given below:

$$\underset{x_{\text{j}},\Delta P_{\text{G,j}},\Delta P_{\text{slk}}}{\text{minimize}} \quad \sum_{j=1}^{N_{\text{d}}} c_{\text{L,j}} x_{\text{j}} P_{\text{L,j}} + \sum_{j=1}^{N_{\text{G}}} c_{\text{G,j}} |\Delta P_{\text{G,j}}| \tag{8}$$

$$\text{subject to} \quad \sum_{j=1}^{N_{\text{d}}} \bar{x}_{\text{j}} P_{\text{L,j}} + P_{\text{C}} - \sum_{j=1}^{N_{\text{G}}} (P_{\text{G,j}} + \Delta P_{\text{G,j}}) = P_{\text{slk}} + \Delta P_{\text{slk}} \tag{9}$$

$$\Delta P_{\text{G,j}}^{\text{down}} \le \Delta P_{\text{G,j}} \le \Delta P_{\text{G,j}}^{\text{up}}, \ \forall\, j, \tag{10}$$

$$\Delta P_{\text{G,j}} = P_{\text{G,j}}(t) - P_{\text{G,j}}(t_0), \ \forall\, j, \tag{11}$$

$$\Delta P_{\text{slk}} = P_{\text{slk}}(t) - P_{\text{slk}}(t_0), \tag{12}$$

$$x_{\text{j}} \in \{0, 1\}, \ \forall\, j \tag{13}$$

$$\bar{x}_{\text{j}} = 1 - x_{\text{j}}, \ \forall\, j, \tag{14}$$

where $c_{\text{L,j}}$ and $c_{\text{G,j}}$ are the participation unit costs for the j^{th} controllable load and the j^{th} GFL inverter in the NLU, respectively. x_j is the switch ON/OFF signal of the j^{th} controllable load. $P_{\text{L,j}}$ and $P_{\text{G,j}}$ are the active powers of the j^{th} controllable load and the base active power rating of the j^{th} GFL inverter, respectively. $\Delta P_{\text{G,j}}$, $\Delta P_{\text{G,j}}^{\text{up}}$ and $\Delta P_{\text{G,j}}^{\text{down}}$ are the computed optimal headroom, and upward and downward headroom limits of the j^{th} GFL inverter, respectively. t and t_0 are the current time instant and the time instant when the contingency happens, respectively. $P_{\text{slk}}(t_0)$ and $P_{\text{C}}(t_0)$ are the active power capacity of the combined *slack bus* and uncontrollable load, respectively, at time instant t_0. ΔP_{slk} is the total active power change of the *slack bus*.

C. HOV ENGINE FOR SUSTAINABLE OPERATION

Considering a grid interruption event and the CI is working in off-grid mode while being supported by its own available backup sources. The objective of the HoV engine is to sustain a viable operation of the CI for a longer time horizon by supplying critical, sub-critical, and non-critical loads by using only the available backup DERs. A trivial solution for the microgrid is to shut down all the sub- and non-critical loads of the CI and use the available DERs to supply only the critical loads (existing brute-force method of the EPSS of the CI); however, this might lead to a reduced quality of service in the CI due to no sub- and non-critical loads being served. Hence, there is a need to devise an optimal scheduling policy for the net-load resources in the CI. To achieve this objective, the optimization algorithm of the HoV engine determines a portfolio of generation and loads to guarantee the viability of all the critical loads while maximizing the level of service of the sub- and non-critical loads in the CI over a given time horizon [30].

A CI contains a collection of net-load resources: n_{d} controllable loads (i.e. sub- and non-critical loads), n_{c} non-controllable loads (i.e., critical loads); n_{g} diesel generator sets; n_{p} GFL solar inverter systems; n_{b} GFM battery inverter systems and a slack bus (combination of all the GFM inverter systems in the CI) to maintain stable voltage and frequency. Let $P^{\mathrm{t}}_{\mathrm{r_j}}$ denote the power output of the j^{th} grid-following solar inverter system at time t. The power delivered by the j^{th} diesel generator set and j^{th} GFL battery inverter system at time t are denoted by $P^{\mathrm{t}}_{\mathrm{g_j}}$ and $P^{\mathrm{t}}_{\mathrm{b_j}}$, respectively. Power delivered by the slack bus at time t is denoted by $P^{\mathrm{t}}_{\mathrm{s}}$. Here, each GFL battery inverter system, j, is characterized by maximum available energy capacity, $E_{\mathrm{b_j}}$, and maximum discharging, $W_{\mathrm{b_j}}$, and charging, $-W_{\mathrm{b_j}}$, power transfer rates. The maximum power dispatch capacity of the j^{th} diesel generator set and the slack bus are denoted by $W_{\mathrm{g_j}}$ and W_{s}, respectively. The maximum available energy in the diesel generator, j, is denoted by $E_{\mathrm{g_j}}$.

The HoV engine solves a convex optimization problem at each discrete time-instant, t_0, to determine the net-load scheduling decisions at some future time instant, t_0+t, where $t \in \{1, 2, \ldots, T\}$, with T being the horizon length. Denote by $x^{\mathrm{t}} := [x^{\mathrm{t}}_1, \ldots x^{\mathrm{t}}_{\mathrm{n_d}}] \in \{0,1\}^{n_{\mathrm{d}}}$, $P^{\mathrm{t}}_{\mathrm{g}} = [P^{\mathrm{t}}_{\mathrm{g}_1}, \ldots P^{\mathrm{t}}_{\mathrm{g}_{n_{\mathrm{g}}}}] \in \mathbb{R}^{n_{\mathrm{g}}}$, $P^{\mathrm{t}}_{\mathrm{b}} = [P^{\mathrm{t}}_{\mathrm{b}_1}, \ldots P^{\mathrm{t}}_{\mathrm{b}_{n_{\mathrm{b}}}}] \in \mathbb{R}^{n_{\mathrm{b}}}$, and $P^{\mathrm{t}}_{\mathrm{s}} \in \mathbb{R}$, $\mathbb{T}_{t_0} := \{t_0, \ldots, T + t_0 - 1\}$. $s^{\mathrm{t_0}}_{\mathrm{g_j}}$ and $s^{\mathrm{t_0}}_{\mathrm{b_j}}$ are the state-of-energy (SOE) and state-of-charge (SOC) of the diesel generator set and the GFL battery inverter systems respectively, at time t_0. Let $\tilde{s}^{\mathrm{t_0}}_{\mathrm{b_j}} := -(1 - s^{\mathrm{t_0}}_{\mathrm{b_j}})$. The optimization problem is given by:

$$
\begin{aligned}
&\underset{\pi}{\text{minimize}} \quad \mathcal{C}(x, p_{\mathrm{g}}, p_{\mathrm{b}}, s^{\mathrm{t_0}}_{\mathrm{b}}, s^{\mathrm{t_0}}_{\mathrm{g}}),\\
&\text{subject to} : 0 \le \textstyle\sum_{t=t_0}^{T+t_0-1} P^{\mathrm{t}}_{\mathrm{g_j}} \le s^{\mathrm{t_0}}_{\mathrm{g_j}} E_{\mathrm{g_j}},\\
&\qquad\qquad \text{for } j = 1, \ldots, n_{\mathrm{g}},\\
&\qquad \tilde{s}^{\mathrm{t_0}}_{\mathrm{b_j}} E_{\mathrm{b_j}} \le \textstyle\sum_{t=t_0}^{T+t_0-1} P^{\mathrm{t}}_{\mathrm{b_j}} \le s^{\mathrm{t_0}}_{\mathrm{b_j}} E_{\mathrm{b_j}},\\
&\qquad\qquad \text{for } j = 1, \ldots, n_{\mathrm{b}},\\
&0 \le P^{\mathrm{t}}_{\mathrm{g_j}} \le W_{\mathrm{g_j}},\\
&\qquad\qquad \text{for } j = 1, \ldots, n_{\mathrm{g}}, t \in \mathbb{T}_{\mathrm{t_0}},\\
&-W_{\mathrm{b_j}} \le P^{\mathrm{t}}_{\mathrm{b_j}} \le W_{\mathrm{b_j}},\\
&\qquad\qquad \text{for } j = 1, \ldots, n_{\mathrm{b}}, t \in \mathbb{T}_{\mathrm{t_0}}\\
&0 \le P^{\mathrm{t}}_{\mathrm{s}} \le W_{\mathrm{s}},\\
&\qquad\qquad \text{for } t \in \mathbb{T}_{\mathrm{t_0}},\\
&\textstyle\sum_{j=1}^{n_{\mathrm{d}}} x^{\mathrm{t}}_{\mathrm{j}} \hat{P}^{\mathrm{t}}_{\mathrm{L_j}} + \sum_{j=1}^{n_{\mathrm{c}}} \hat{P}^{\mathrm{t}}_{\mathrm{c_j}}\\
&= \sum_{j=1}^{n_{\mathrm{g}}} P^{\mathrm{t}}_{\mathrm{g_j}} + \sum_{j=1}^{n_{\mathrm{b}}} P^{\mathrm{t}}_{\mathrm{b_j}}\\
&+ \textstyle\sum_{j=1}^{n_{\mathrm{p}}} \hat{P}^{\mathrm{t}}_{\mathrm{r_j}} + P^{\mathrm{t}}_{\mathrm{s}}, \ \text{for } t \in \mathbb{T}_{\mathrm{t_0}},\\
&x^{\mathrm{t}}_{\mathrm{j}} \in \{0, 1\},\\
&\text{for } j = 1, \ldots, n_{\mathrm{d}}, \ \text{for } t \in \mathbb{T}_{\mathrm{t_0}},
\end{aligned}
$$

where the objective function is:

$$
\begin{aligned}
&\mathcal{C}(x, p_{\mathrm{g}}, p_{\mathrm{b}}, s_{\mathrm{b}}, s_{\mathrm{g}})\\
&= \textstyle\sum_{t=t_0}^{\mathrm{T}+t_0-1} \Big[\sum_{j=1}^{n_{\mathrm{b}}} c_{\mathrm{b_j}}(s^{\mathrm{t_0}}_{\mathrm{b_j}}, P^{\mathrm{t}}_{\mathrm{b_j}})\\
&- \textstyle\sum_{j=1}^{n_{\mathrm{g}}} c_{\mathrm{g_j}}(\eta_{\mathrm{g_j}}(P^{\mathrm{t}}_{\mathrm{g_j}})) + \sum_{j=1}^{n_{\mathrm{d}}} c_{\ell_{\mathrm{j}}}(1 - x^{\mathrm{t}}_{\mathrm{j}}) \hat{P}^{\mathrm{t}}_{L_{\mathrm{j}}} \Big].
\end{aligned}
$$

The dispatch decisions are based on renewable generation forecasts, predicted profiles of the loads in the CI, and information about the latest SOC and SOE (the amount of energy equivalent fuel remaining relative to its reserve capacity), of the GFL battery inverter systems and diesel generator sets, respectively. This process is repeated at the subsequent time instants with updated sets of measurements. More details about the constraints and the objective function design of the HoV engine optimization problem can be found in [30].

V. DESIGNED TEST CASES FOR THE EPSS OF THE CI

This section describes three test cases that are designed based on the challenges and the proposed modifications of the EPSS for the CI.

A. TEST CASE 1:

Test Case 1 is described in Table 1. Test Case 1 is designed to:

- Test the capability of having seamless transitions from on-grid to off-grid mode of the CI after a grid interruption with the help of the proposed modification in the GFM inverters, as described in Section IV-A, while serving critical loads.
- Test the operation of the CI with successive increases in generation through the available diesel generation sets and by serving more critical loads while maintaining stringent power qualities and regulations with the NLM engine, as described in Section IV-B.
- Test the capability of the CI to prioritize critical loads with the NLM engine, as described in Section IV-B, when solar irradiance is reduced while maintaining standard power qualities and regulations.

TABLE 1. Test case designed to demonstrate the capability of the proposed epss for a ci to have seamless transitions from on-grid to off-grid mode after grid failure and viable operation by serving critical loads via local energy resources.

Time [s]	Primary Source	Load Condition	Event Description
$t = 0$	Grid + PV GFL Inverter = 33kVA	Critical Load = 233kVA +Non-critical Load = 266kVA	Initial Condition • Grid and PV inverter supplies the entire load of the CI. • GFM Inverters are always connected to not supplying power. Occurrence of Event • Anomaly in grid is detected, grid disconnected.
$t = t_1$	Battery GFM Inverter = 133kVA + PV GFL Inverter = 33kVA	Critical Load = 166kVA	Initial Condition • Diesel Gen − Sets are brought back online Occurrence of Event • Seamlessly transferring the load from ongrid to offgrid • achieve generation demand balance by NLM Engine.
$t = t_2$	Battery GFM Inverter = 133kVA + PV GFL Inverter = 33kVA + Diesel Gen − Set = 67kVA	Critical Load = 233kVA	Initial Condition • Battery, PV Inverters are supplying loads initially. • Diesel Gen Sets achieve synchronous speed. Occurrence of Event • Diesel Gen-Sets connected, power balance by NLM.
$t = t_3$	Battery GFM Inverter = 133kVA + PV GFL_Inverter = 6.7kVA + Diesel Gen − Set = 67kVA	Critical Load = 206.7kVA	Initial Condition • Battery, PV Inverters and Diesel Gensupply loads initially. Occurrence of Event • Solar irradiance decreases, curtailing loads by NLM.

TABLE 2. Test case designed to demonstrate the capability of the proposed epss for a ci to have black-start operation and viable operation by serving critical loads via local energy resources.

Time [s]	Primary Source	Load Condition	Event Description
$t = 0$	Battery GFM Inverter = 133kVA + PV GFL Inverter = 33kVA	Critical Load = 166kVA	Initial Condition • CI is in off − grid mode and completely de − energized. Occurrence of Event • Black − start by GFM, PV and NLM engine
$t = t_1$	Battery GFM Inverter = 133kVA + PV GFL Inverter = 33kVA + Diesel Gen − Set = 67kVA	Critical Load = 233kVA	Initial Condition • Diesel Gen Sets are slow to achieve synchronous speed Occurrence of Event • Diesel Gen Sets brought online, NLM increases loads.
$t = t_2$	Battery GFM Inverter = 133kVA + PV GFL Inverter = 33kVA + Diesel Gen − Set = 67kVA + Mobile Inverter = 67kVA	Critical Load = 300kVA	Initial Condition • Diesel Gen Sets, GFM and PV supply loads initially. Occurrence of Event • Mobile GFL brought online, NLM increases loads.
$t = t_3$	Battery GFM Inverter = 133kVA + PV GFL Inverter = 33kVA + Mobile Inverter = 67kVA	Critical Load = 233kVA	Initial Condition • Diesel Gen Sets, GFM, PV and Mobile GFL supply load Occurrence of Event • Diesel Gen Sets are tripped, curtailing load by NLM.
$t = t_4$	Grid + PV GFL Inverter = 33kVA	Critical Load = 233kVA +Non-critical Load = 266kVA	Initial Condition • Diesel Gen Sets, GFM, PV and Mobile GFL supply load Occurrence of Event • Grid returns, GFMs connected, not supplying power.

B. TEST CASE 2

Test Case 2 is described in Table 2. Test Case 2 is designed to:

- Test the capability of the EPSS to black-start the CI using local generation sources and using the fast-acting NLM engine, as described in Section IV-B, while maintaining stringent power qualities and regulations.
- Test the capability of the CI to demonstrate the performance of the NLM engine in tackling contingencies, such as tripping diesel generation sets, while maintaining power qualities and regulations according to standards.
- Test the capability of having seamless transitions from off-grid to on-grid mode of the CI after the grid is restored with the help of the proposed modification in the GFM inverters.

C. TEST CASE 3

Test Case 3 is designed to:

TABLE 3. Metrics on voltage, frequency regulation limits and power quality measures.

Metric Type		Metric Value
Regulation Limit	Frequency range	$\leq \pm 0.5$ Hz
	Voltage range	$\leq \pm 10\%$ pu
Power Quality Limit	THD in voltage	$\leq 8\%$ pu
	Individual distortion	$\leq 5\%$ pu

- Test the capability of the EPSS to operate the CI for a longer time horizon using the proposed HoV engine, as described in Section IV-C, compared with the Base Case engine, as described in Section V-A of [26].
- Showcase the advantage of the proposed HoV engine in the EPSS over the existing Base Case engine.

To evaluate the performance of the developed HoV engine, the following metrics are defined:

Total remaining energy (TRE) The TRE (in kWh) of the DERs in the CI (i.e., battery inverters and diesel generators)

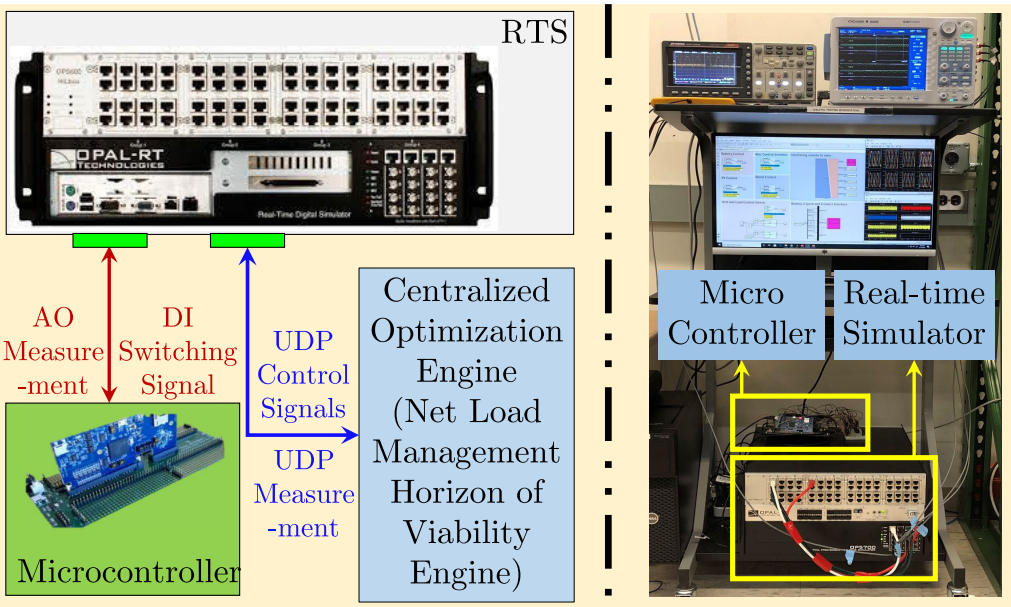

FIGURE 5. Controller-hardware-in-the-loop simulation set-up with real-time simulator interfaced with physical micro-controllers and server workstations.

at the end of the time horizon $[0, \mathcal{T}]$ is defined as:

$$\mathrm{TRE}(\mathcal{T}) := \sum_{j=1}^{n_\mathrm{g}} s_{\mathrm{g}_j}^{\mathcal{T}} E_{\mathrm{g}_j} + \sum_{j=1}^{n_\mathrm{b}} s_{\mathrm{b}_j}^{\mathcal{T}} E_{\mathrm{b}_j}. \tag{15}$$

Cost-weighted energy (CWE) The total CWE delivered to all critical and deferrable loads in the microgrid over a time horizon $[0, \mathcal{T}]$ is defined as:

$$\mathrm{CWE}(\mathcal{T}) := \int_0^{\mathcal{T}} \mathrm{CWP}\, \mathrm{d}t = \int_0^{\mathcal{T}} \sum_{i=1}^{n_\mathrm{d}+n_\mathrm{c}} c_{\ell_i} P_{\mathrm{L}_i}^{\mathrm{t}}\, \mathrm{d}t, \tag{16}$$

where CWP is the cost-weighted power delivered; and $P_{\mathrm{L}_i}^{\mathrm{t}}$ is the per-unit power of load, i. The metrics in (15) and (16) capture the trade-off between the guaranteed viability of power for the CI units (higher remaining energy implies the availability of more energy in the generation resources of the CI units) and the level of service of the required loads of the CI (higher CWE implies that more higher-priority loads are running). Note that the performance of the proposed EPSS system in all three test cases will be examined based on the accredited standards on voltage and frequency regulation limits and power quality measures, i.e., total harmonic distortion (THD) and individual harmonic distortion, as recommended by [5] and [38] as tabulated in Table 3.

VI. CHIL-BASED VALIDATION AND RESULTS

A. CHIL CONFIGURATION

A CHIL-based real-time (RT) simulation studies are conducted on a test-system under study that is developed based on the electrical network of a commercial-scale medical center [40]. The CI shown in Fig. 1 is an R-L network of 3-ϕ, 60Hz, 480V (line-to-line), and it has critical loads of 150kW, 72kVAr; sub-critical loads of 60kW, 30kVAr; and non-critical loads of 240kW, 115kVAr. The main feeder and the DERs of the CI are tabulated in Table 4. The entire CI network with the grid and DERs is emulated inside the OP5700 real-time simulator (RTS) manufactured by OPAL-RT using the eMEGASIM platform for electromagnetic transient simulation. The control loops of one GFL solar inverter system and one GFM battery inverter system are realized on two Texas Instruments TMS320F28379D, 16/12-bit floating-point 200MHz Delfino microcontroller boards. The NLM and HoV optimization engines are implemented on a server workstation, developed using Python 3.7.1, with commercial optimization solver, MOSEK. A device control gateway is realized using standard User Datagram Protocol (UDP), which emulates the communication layer for continuously listening to the measurements sent from the RTS and dispatching commands from the NLM/HoV engine to the RTS, as shown in Fig. 5. The CHIL experiment is conducted to evaluate the performance in Test Case 1, Test Case 2, and Test Case 3, and results are discussed next.

B. CHIL SIMULATION-BASED VALIDATION AND RESULTS

The CHIL-based validation of Test Case 1 for 360s and corresponding results are shown in Fig. 6. The active and reactive power output of GFM battery-supported inverters are shown in Fig. 6(a), Fig. 6(b), respectively. Fig. 6(c), and Fig. 6(d) show the active and reactive power outputs of the grid and solar GFL inverter, respectively. It is observed that all the critical, sub-critical and non-critical loads of the CI are supplied by the grid and the solar GFL inverter alone in on-grid mode. With the help of the modified

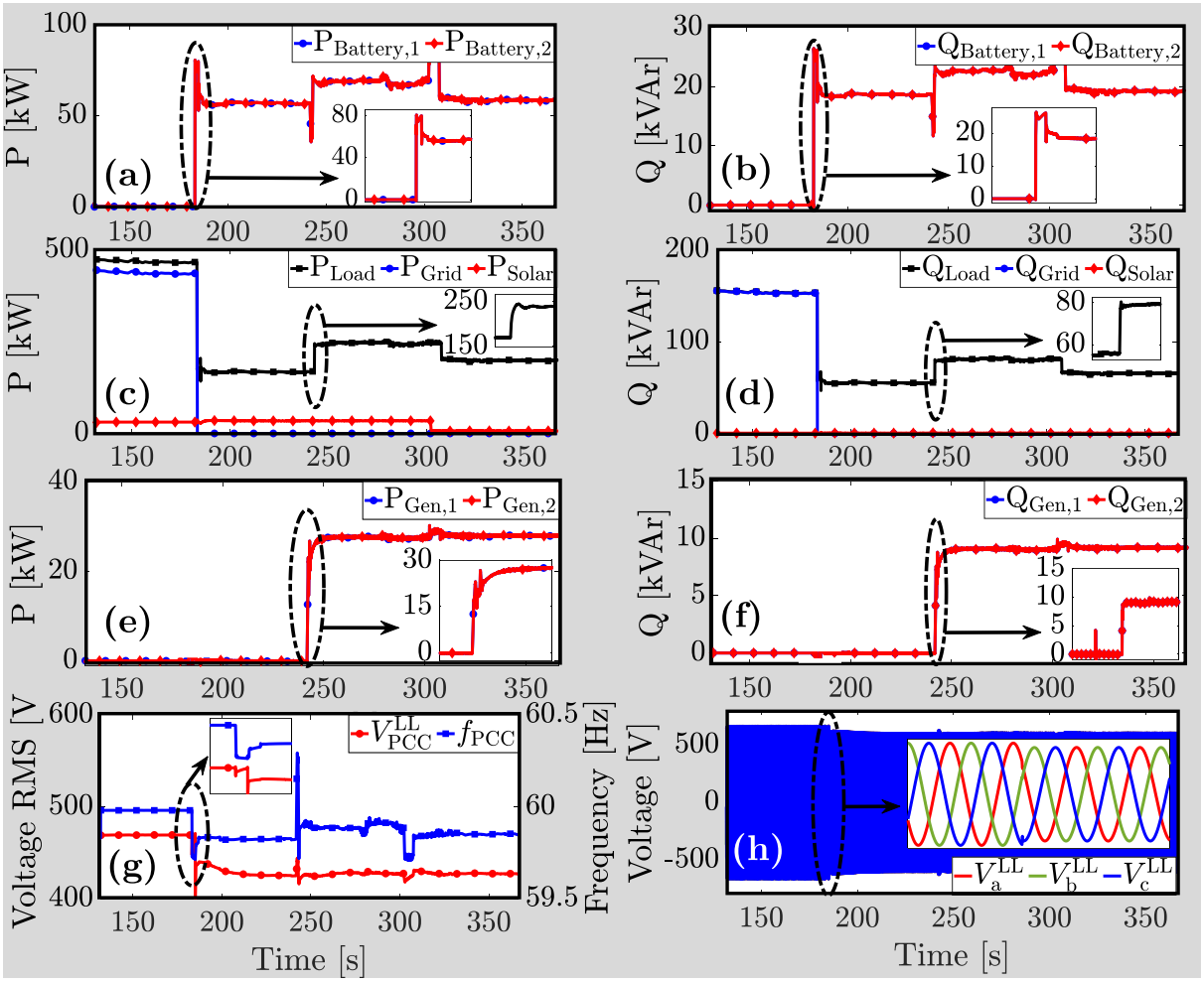

FIGURE 6. CHIL results of (a) active power output, (b) reactive power output of GFM battery inverter systems, (c) active power output, (d) reactive power output of the grid, loads, and solar inverter system, (e) active power output, (f) reactive power output of the diesel generation sets, (g) line-to-line voltage RMS and frequency, (h) instantaneous voltage waveform measured as emergency bus of the CI system of Fig. 1 during Test Case 1 of Table 1.

TABLE 4. 3-Phase parameters of grid feeder and DERs of the CI.

Inverter	Value of the Parameters
Ratings (3-ϕ)	480 V (L-L), 60 Hz, 125 kVA, 0.85 pf
DC Side	V_{dc} = 850 V, f_{sw} = 10 kHz
LCL Filter	L_f = 150 μH, L_g = 15 μH, C_f = 110 μF
Droop Control	n_i=4 $\frac{mHz}{kW}$, m_i=0.2 $\frac{volt}{kVAr}$, k_i=0.67 $\frac{volt/s}{kVAr}$
GFM Control	$k_{pc,i}$=0.45, $k_{ic,i}$=150, $k_{pv,i}$=0.1, $k_{iv,i}$=37.1,
GFL Control	PLL's PI Regulator: k_p^{pll}=0.05, k_i^{pll}=0.5
Diesel Set	**Value of the Parameters**
Ratings (3-ϕ)	480 V (L-L), 60 Hz, 135 kVA, 0.85 pf
Droop Control	n_g(P-f) = 4 mHz/kW, m_g(Q-V) = 0.2 V/kVAr
Grid	**Value of the Parameters**
Ratings (3-ϕ)	13.8 kV fed Y-Y 0.75 MVA, 13.8/0.48 kV Xr.
Feeder Line	$R_{l,g}$ = 5 mΩ, $L_{l,g}$ = 30 μH

droop law employed to GFM inverters, the EPSS achieves seamless transition from on-grid to off-grid mode around t $\approx$ 180s. The diesel generation sets are brought online and synchronized after time $t_2 \approx 250s$; Fig. 6(e) and Fig. 6(f) show the active and reactive power output of diesel gen-set, respectively. At $t_3 \approx 300s$, the output power of the solar inverter curtails due to low irradiance. The NLM engine performs a fast-acting control to increase/decrease loads to maintain balance between generation and demand. Similarly, the CHIL-based validation of Test Case 2 for 540s and the corresponding results are shown in Fig. 7. The active and reactive power output of GFM battery-supported inverters are shown in Fig. 7(a), and Fig. 7(b). Fig. 7(c), and Fig. 7(d) show the active and reactive power outputs of the grid and solar GFL inverter, respectively. The NLM engine is making sure to supply the major critical load and some sub-critical loads during the initial black start condition and increases the load when the diesel generation sets are brought online at $t_1 \approx 300s$ and the GFL mobile battery inverter system is synchronized at $t_2 \approx 360s$, as shown in Fig. 7(e) and Fig. 7(f), respectively and decrease load at $t_3 \approx 420s$ when the diesel generation sets are disconnected due to exhausting the fuel limits. At $t_4 \approx 480s$, the grid returns, and the entire load is supplied alone by the grid and solar GFL inverter

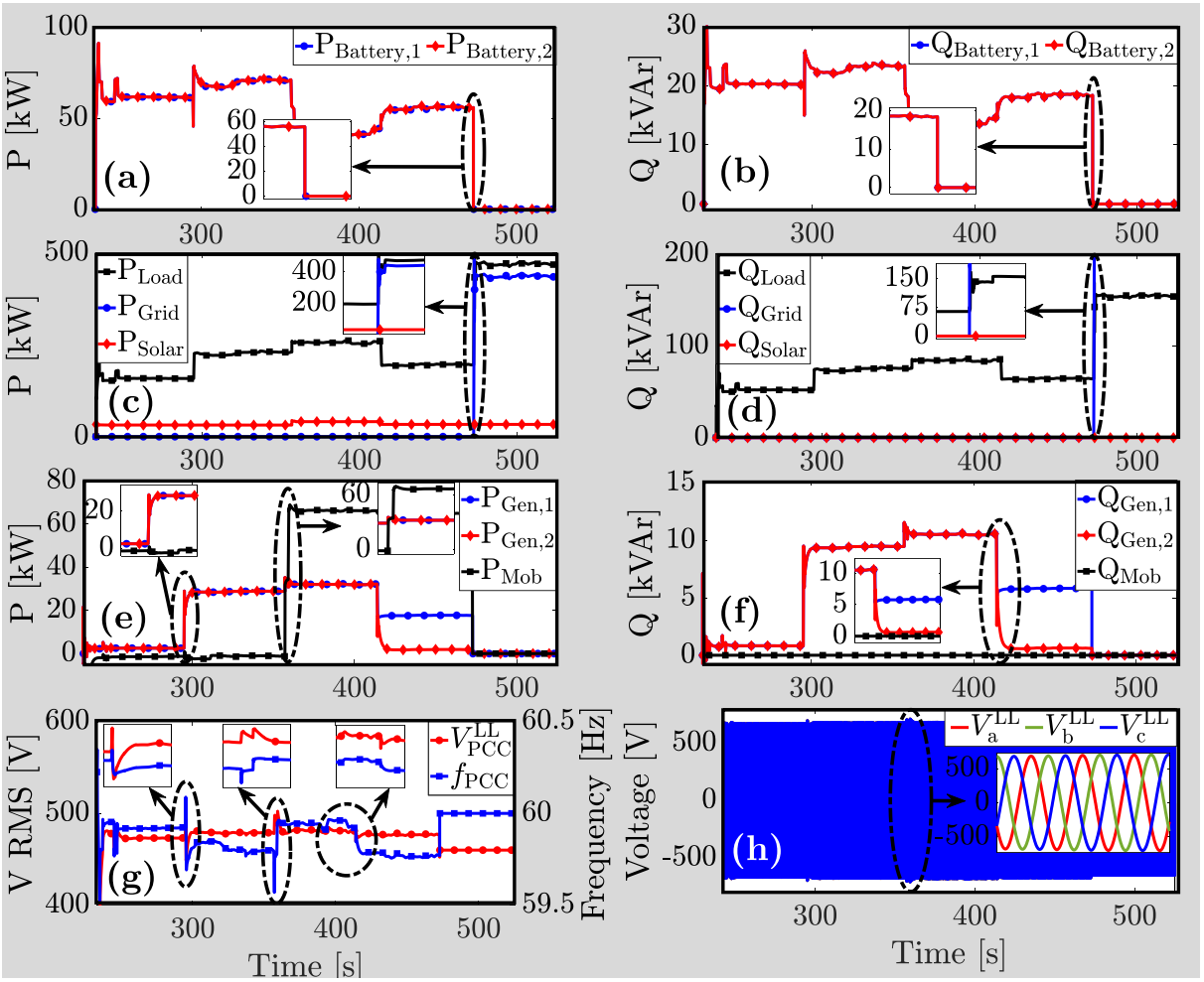

FIGURE 7. CHIL results of (a) active power output, (b) reactive power output of GFM battery inverter systems, (c) active power output, (d) reactive power output of the grid, loads, and solar inverter system, (e) active power output, (f) reactive power output of the diesel generation sets and mobile grid-following inverter system, (g) line-to-line voltage RMS and frequency, (h) instantaneous voltage waveform measured as emergency bus of the CI system of Fig. 1 during Test Case 2 of Table 2.

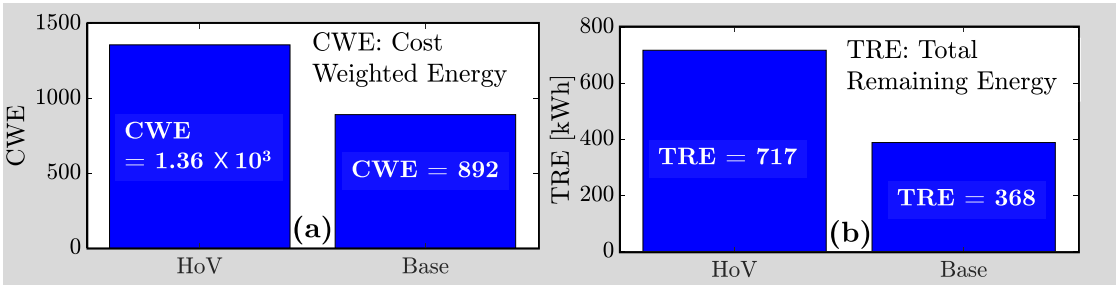

FIGURE 8. Comparative results of (a) total cost-weighted energy and (b) total remaining energy (in kWh), resulting from HoV engine and base case engine during 1 hours of the CHIL experiment on the test system of Fig. 1.

system. Fig. 6(g), Fig. 6(h), Fig. 6(g), and Fig. 6(h) show the voltage RMS, the system frequency, and the instantaneous voltage measured at the emergency bus during Test Case 1 and Test Case 2, respectively and it is observed that all the metrics, as tabulated in Table 3, are satisfied during both test cases. Note that the GFM inverters, which are still connected to the emergency bus, have regulated the output active and reactive power by the enhancement in the droop curve, as mentioned in Section IV-A, once the grid comes online.

Figs. 8 demonstrates the performance of the HoV engine compared to the Base Case with respect to the TRE and CWE

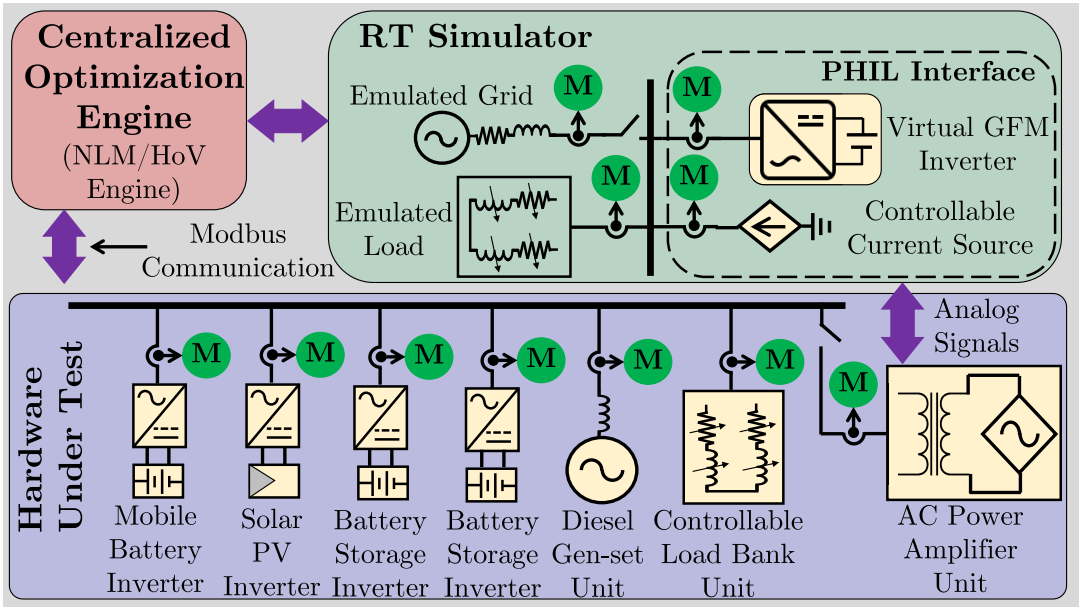

(a)

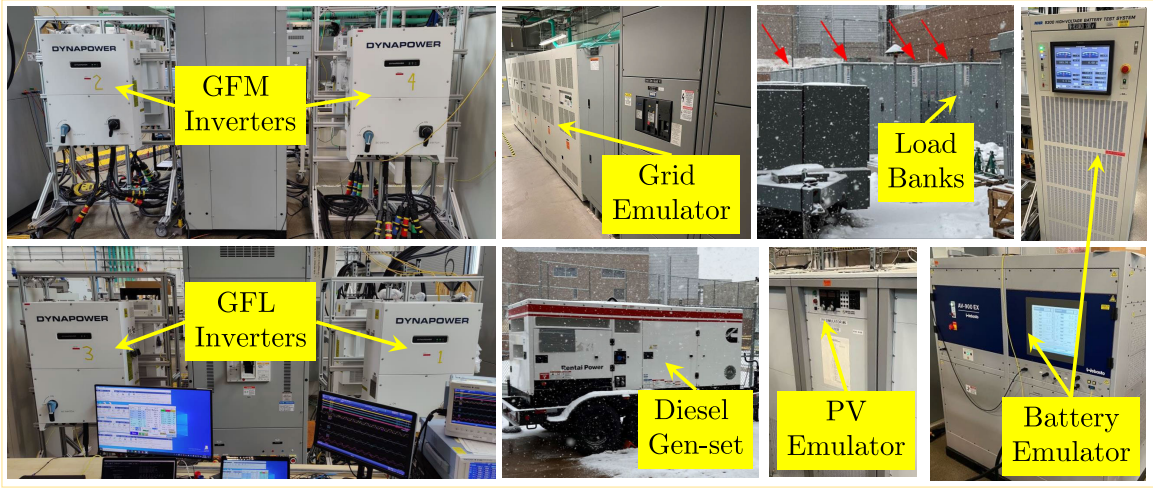

(b)

FIGURE 9. The diagram of (a) the entire power-hardware-in-the-loop configuration of the test system under study, (b) laboratory-based at-scale hardware setups with various types of sources and loads.

metrics, in (15) and (16), respectively. Fig. 8(a) demonstrates that the HoV engine provides more total CWE than the Base Case engine during the 1-hour horizon; therefore, the HoV engine provides power to more high-priority critical and sub-critical loads in a resource-constrained scenario during the time duration of the experiment. Fig. 8(b) provides a comparison based on the TRE. The HoV optimization engine optimally schedules the available generation sources that result in a higher TRE available at the end of 1 hour that can be used to serve the critical and sub-critical loads in the CI at a later time instant. This shows the advantage of the proposed HoV engine over the existing Base Case engine in the sense of extending the horizon of the viable operation of the CI. It is observed that, initially the HoV engine is inclined toward running more load in the CI, which is similar to Base Case engine; therefore, initially, the HoV engine is aggressive in terms of maintaining a good quality of service to the load, but it adjusts to conserve generation for future times of operation. During the end of the time horizon, when the SOC level of the batteries is low, the HoV engine jumps to a more energy-saving mode compared to the Base Case engine.

VII. PHIL BASED VALIDATION AND RESULT

A. PHIL CONFIGURATION

The PHIL-based experimental configuration and the large-scale laboratory-based hardware systems are shown in

TABLE 5. Resulting values of the metrics on voltage, frequency regulation limits, and power quality measures in PHIL.

Metric		TC 1	TC 2	TC 3
Freq.	Max[↑]	+0.03 Hz	+0.05 Hz	+0.04 Hz
Range	Max[↓]	−0.31 Hz	−0.32 Hz	−0.29 Hz
Volt.	Max[↑]	+0.9%	+0.8%	+0.9%
Range	Max[↓]	−8.9%	−8.1%	−9.2%
THD	Max	6.3%	6.8%	6.7%
Volt.	Min	1.1%	1.5%	1.9%
Ind.	Max	4.3%	4.9%	4.7%
Dist.	Min	0.9%	1.2%	1.4%

Fig. 9(a) and Fig. 9(b). The hardware under test of the PHIL setup has the following components:

1) two 3-ϕ, 125-kVA, 4-quadrant GFM inverters, manufactured by Dynapower; interfaced with Aerovironment AV-900 and NH Research 9300 bidirectional battery storage systems,

2) two 3-ϕ, 125-kVA, 4-quadrant GFL inverters, manufactured by Dynapower, two interfaced with Magna Power MT250-1000 unidirectional battery and PV emulator systems,

3) four 3-ϕ, 250-kW LoadTec OSW4C-based load banks,

4) one 3-ϕ, 135-kW Cummins C150D2RE diesel genset.

The control parameters of the GFM inverter, GFL inverter, and diesel generation units are tabulated in Table 4. The PHIL interface consists of the following:

1) one 3-ϕ, 270-kVA Ametek RS-series power amplifier,

2) three LEM DVL750 voltage transducers,

3) three LEM LF-350-S current transducers.

An Opal RT OP5700-series real-time simulator with a time step of $T_s = 50\mu s$ is used to execute the in-the-loop system, which consists of *P-Q* loads, the emulated grid, and a novel PHIL interface control block, as discussed in [41], which consists of a virtual GFM inverter model and three discrete-time PHIL interface compensators. The parameters of the controller and the power circuit of the virtual inverter are similar to the physical GFM inverter system under study with the same control parameters as tabulated in Table 4. PHIL experiment is conducted to evaluate the performance of Test Case 1 and Test Case 2, and, results are discussed next.

B. PHIL SIMULATION-BASED VALIDATION AND RESULTS

The PHIL-based validation of Test Case 1 for 300s and the corresponding results are shown in Fig. 10. The active and reactive power flow of both physical and virtual GFM battery-based inverter systems during the events of Test Case 1 are shown in Fig. 10(a) and Fig. 10(b), respectively. As emphasized in the figures, the enhanced droop control for the GFM inverters, as described in Section IV-A, enables the EPSS to achieve seamless transition capability from on-grid to off-grid mode ($t_1 \approx 100s$) with substantially less transients. Moreover, during on-grid mode, the output active and reactive power of both GFM inverters are regulated to the desired value (in this case, zero); therefore, during on-grid mode, all the critical, sub-critical, and non-critical loads of the CI are supplied by the grid and the solar inverter system alone, as shown in Fig. 10(c) and Fig. 10(d) respectively. With this seamless transition to off-grid mode, however, the GFM inverters along with the solar inverter systems supply the critical loads and some sub-critical loads based on the decision made by fast-acting NLM engine, as mentioned in Section IV-B. The NLM engine is able to make the decision of optimal loading based on available generation within 96ms. Diesel generation sets are brought online and synchronized after time $t_2 \approx 180s$, as shown in Fig. 10(e) and Fig. 10(f), respectively. Eventually, the NLM engine decides to add and supply more critical loads due to the increase in the available generation capability of the EPSS and is able to make the decision within 97ms. Moreover, at $t_3 \approx 240s$, the output power of the solar inverter curtails due to low irradiance, and the fast-acting NLM engine takes care of the contingency situation by curtailing some sub-critical loads to maintain balance between generation and demand. It is observed that during every contingencies, the fast acting NLM engine is able to find the optimal solution of loading by 100ms based on generation capability.

Similarly, the PHIL-based validation of Test Case 2 for 300s and the corresponding results are shown in Fig. 11. The active and reactive power flow of both the physical and virtual GFM battery-based inverter systems during the events of Test Case 2 are shown in Fig. 11(a) and Fig. 11(b), respectively. With the advanced and fast-acting NLM engine decision within 97.14ms and GFM capability, the major critical load and some sub-critical loads are being supplied during the initial black-start condition. The diesel generation sets are brought online and synchronized at time $t_1 \approx 65s$, as shown in Fig. 11(e) and Fig. 11(f), respectively. Eventually, the NLM engine decides to add and supply more critical loads due to the increase in the available generation capability of the EPSS and the decision is made by 95ms. Moreover, at $t_2 \approx 120s$, the GFL mobile battery inverter system is synchronized and connected, and as a result, the fast-acting NLM engine adds and supplies more critical and sub-critical loads, as shown in Fig. 11(c) and Fig. 11(d), respectively. At $t_3 \approx 180s$, the diesel generation sets are disconnected as they exhaust the fuel limits, and the NLM engine tackles the contingency situation by curtailing some loads to maintain balance between generation and demand. In this major contingency, the NLM engine completes the optimal solution by 95ms. At $t_4 \approx 240s$, the grid returns, and all the loads of the CI are supplied alone by the grid and solar inverter system once the grid is synchronized and connected to the CI. Note that the GFM inverters, which are still connected to the emergency bus, have regulated output active and reactive power by the enhancement in the droop curve, as mentioned in Section IV-A, once the grid comes back online.

Figs. 12 demonstrate the performance of the HoV engine compared to the Base Case with respect to the ratio of TRE and CWE metrics as mentioned in (15) and (16) respectively. These two figures show the run time ratios of

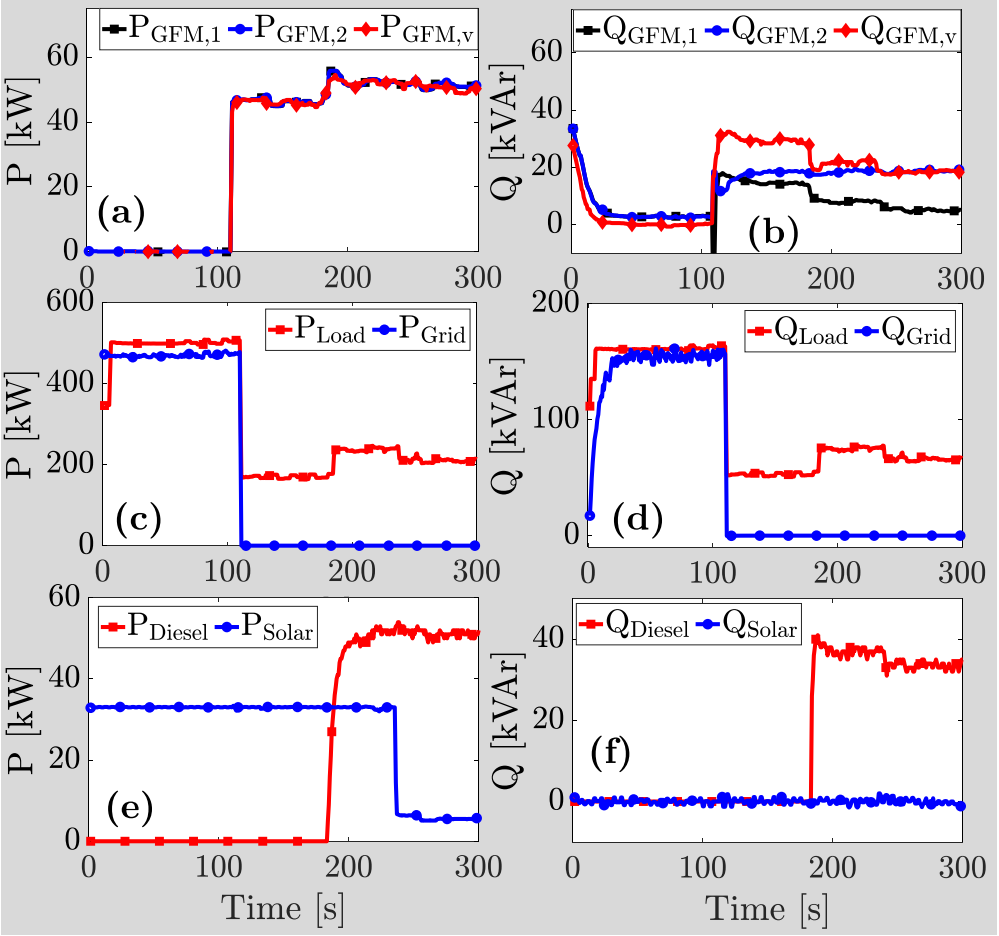

FIGURE 10. PHIL results of (a) active power output, (b) reactive power output of GFM battery inverter systems, (c) active power output, (d) reactive power output of the grid, loads, and solar inverter system, (e) active power output, (f) reactive power output of the diesel generation sets of the CI system of Fig. 1 during Test Case 1 of Table 1.

the CWE and TRE metrics (ρ_{CWE} and ρ_{TRE}). Fig. 12(a) demonstrates that the HoV engine provides more total CWE than the base case engine over the 1 hour horizon (the ratio is more than 1); therefore, the HoV engine provides power to more high-priority critical and sub-critical loads in a resource-constrained scenario during the time duration of the experiment. Fig. 12(b) provides a comparison based on the total remaining energy. The HoV optimization engine optimally schedules the available generation sources that result in a higher total remaining energy available at the end of 1 hours that can be utilized to serve the critical and sub-critical loads in the CI at a later time instant. This shows the advantage of the proposed HoV engine over the existing base case engine in the sense of extending the horizon of the viable operation of the CI. It is observed that initially the HoV engine is inclined toward running more load in the CI that is similar to base case engine. Therefore, initially, the HoV engine is aggressive in terms of maintaining a good quality of service to the load, but it adjusts itself to conserve generation for future times of operation. However, during the end of the time horizon, when the SOC level of the batteries are low, the HoV engine jumps to more energy saving mode compare to the base case engine case. It can be observed that the HoV engine is equally conservative in restoring the energy of the batteries in the CI but more aggressive in terms of supplying a higher number of prioritized loads compared to the base case engine (indicated by $\rho_{\text{CWE}} > 1$ and $\rho_{\text{TRE}} \approx 1$). Yet, toward the end of the horizon, the HoV engine is more aggressive in restoring the energy of the batteries in the CI but equally aggressive in terms of supplying prioritized loads compared to the base case engine (indicated by $\rho_{\text{CWE}} \approx 1$ and $\rho_{\text{TRE}} > 1$).

VIII. DISCUSSIONS ON RESULTS

Based on the initial CHIL-based, and the large scale PHIL-based demonstrations and the corresponding results, the following observations can be made:

1) During on-grid to off-grid and off-grid to on-grid transition of the CI, the integrator in the Q-V droop law ensures that the reactive power output of the GFM

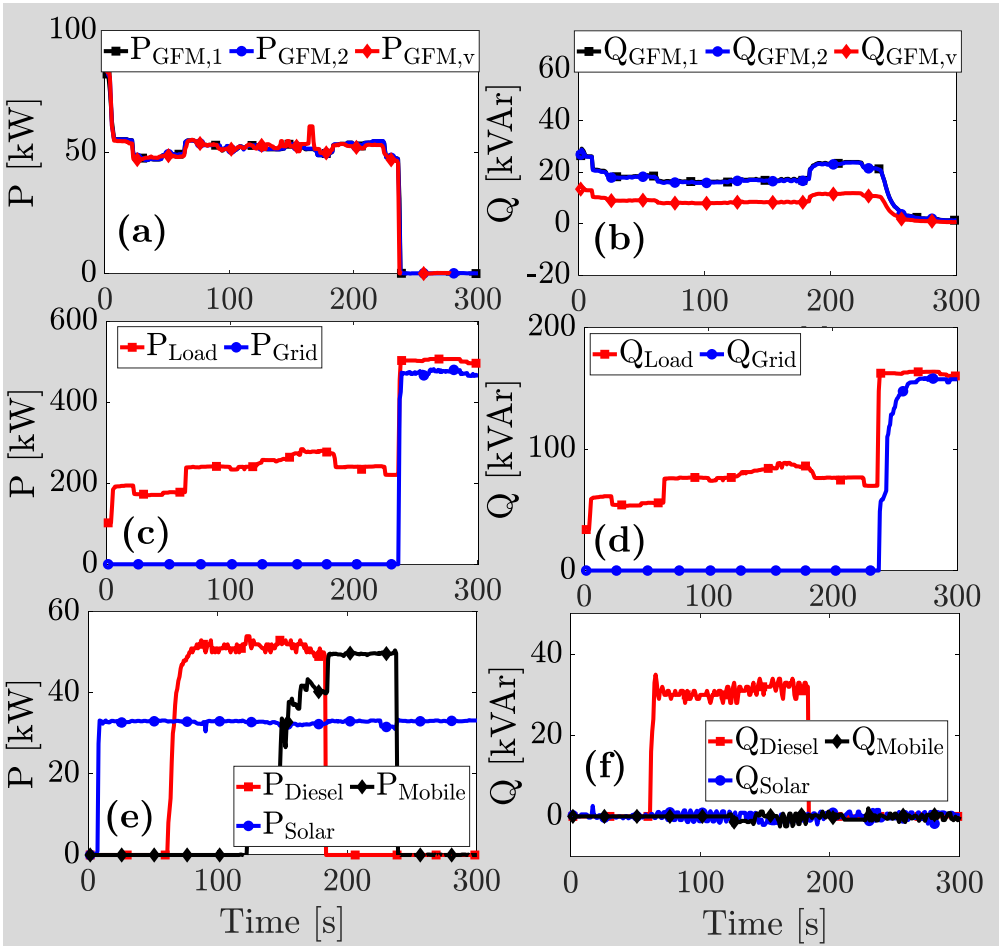

FIGURE 11. PHIL results of (a) active power output, (b) reactive power output of GFM battery inverter systems, (c) active power output, (d) reactive power output of the grid, loads, and solar inverter system, (e) active power output, (f) reactive power output of the diesel generation sets and mobile grid-following inverter system of the CI system of Fig. 1 during Test Case 2 of Table 2.

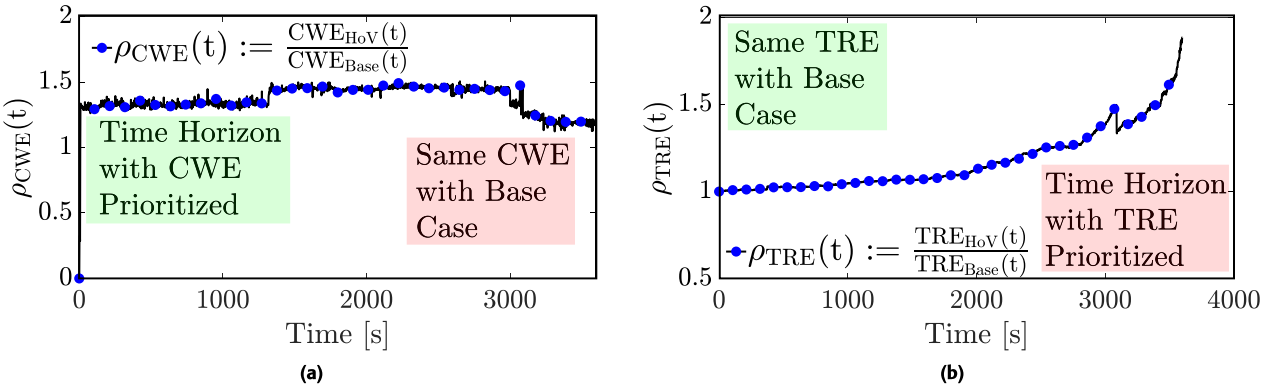

FIGURE 12. Comparative results of (a) the ratio of the CWE metric value resulting from HoV engine and base case engine, (b) ratio of the TRE metric value resulting from HoV engine and base case engine during 1 hours of PHIL experiment on the test system of Fig. 1.

inverters are zero and the P-f droop law ensures the active power output is zero. The experimental data establishes the effectiveness of the always grid-forming operation and control of inverters in meeting power delivery objectives when on-grid and off-grid under various kinds of loads and scenarios while minimizing transients, i.e. frequency is kept under ±0.5 Hz and the voltage is kept under ±10% of the nominal voltage rating, before, after and during transitions. These strict regulations on the frequency and voltage of the system

are well under the limits recommended by IEEE standards [2], [38]. The novel mode-dependent droop controller for the GFM inverters enhances the seamless transition capability of the EPSS that is a significant improvement over the existing solutions for EPSS of CI.

2) During the test cases, various contingencies are tested during the operation of the EPSS of the CI. During major contingencies such as on-grid to off-grid jump, off-grid to on-grid jump, tripping of diesel gen-sets, drop in solar irradiance, etc., the fast-acting NLM engine was always able to maintain the balance in total available generation and the power demand by determining the optimal amount of loads and power set-points of GFL inverters. These optimal decisions were successfully determined within 100 ms during various cases, that is significantly fast in action in comparison with conventional EPSS for CI. The performance of the fast-acting NLM engine during these contingencies corroborate the fact that the operation of the EPSS employed with the NLM engine regulates the voltage and frequency of the system under the strict limit recommended by the grid codes [2], [38]. Table 5 shows that the maximum frequency deviation is -0.32 Hz and the maximum voltage deviation is -9.2% of the nominal voltage during all three test cases. These numbers are well within the recommended limits suggested by IEEE 1547 Std. Moreover, the maximum total harmonic distortion (THD) and the individual harmonic distortion limits of the voltage waveform at emergency bus are 6.7% and 4.9% during all three test cases, that follow the recommendations of the IEEE Std. 519 [42].

IX. CONCLUSION

This article proposes a comprehensive design of the EPSS for the uninterrupted operation of CI by employing various novel techniques, including 1) novel mode-dependent droop-controlled GFM inverters for seamless transition capability; 2) a fast-acting optimal net-load management engine for the efficient and optimal operation of CI; and 3) a novel optimization-based HoV engine for longer, sustained, and viable operation in the aftermath of a grid failure as recommended in the standards. Both CHIL- and PHIL-based studies using defined test cases on the test system based on the realistic electrical network of a commercial-scale medical center are performed in the validation stage. The results corroborate the efficacy and empirical robustness of the proposed strategy for EPSS employed in CI by achieving good regulation limits and power quality measures while considering the enhancements as recommended by the standards.

ACKNOWLEDGMENT

The views expressed in the article do not necessarily represent the views of the DOE or the U.S. Government. The U.S. Government retains and the publisher, by accepting the article for publication, acknowledges that the U.S. Government retains a nonexclusive, paid-up, irrevocable, worldwide license to publish or reproduce the published form of this work, or allow others to do so, for U.S. Government purposes.

REFERENCES

[1] A. B. Smith and R. W. Katz, "U.S. billion-dollar weather and climate disasters: Data sources, trends, accuracy and biases," *Natural Hazards*, vol. 67, no. 2, pp. 387–410, Jun. 2013.

[2] *IEEE Recommended Practice for Electric Systems in Health Care Facilities*, IEEE Standard 602-2007, 2007, pp. 1–436.

[3] *NFPA 99: Standard for health care facilities*, National Fire Protection Association, Quincy, MA, USA, 1996.

[4] *NFPA 110: Standard for Emergency and Standby Power Systems*, National Fire Protection Association, Quincy, MA, USA, 2005.

[5] *IEEE Draft Recommended Practices and Requirements for Harmonic Control in Electric Power Systems*, Standard IEEE P519/D6ba, Sep. 2013, pp. 1–26.

[6] *NFPA 111: Standard on Stored Electrical Energy, Emergency and Standby Power Systems*, National Fire Protection Association, Quincy, MA, USA, 2005.

[7] M. A. Igder, X. Liang, and M. Mitolo, "Service restoration through microgrid formation in distribution networks: A review," *IEEE Access*, vol. 10, pp. 46618–46632, 2022.

[8] X. Liang, M. A. Saaklayen, M. A. Igder, S. M. R. H. Shawon, S. O. Faried, and M. Janbakhsh, "Planning and service restoration through microgrid formation and soft open points for distribution network modernization: A review," *IEEE Trans. Ind. Appl.*, vol. 58, no. 2, pp. 1843–1857, Mar. 2022.

[9] H. Hui, Y. Chen, S. Yang, H. Zhang, and T. Jiang, "Coordination control of distributed generators and load resources for frequency restoration in isolated urban microgrids," *Appl. Energy*, vol. 327, Dec. 2022, Art. no. 120116. [Online]. Available: https://www.sciencedirect.com/science/article/pii/S0306261922013733

[10] A. Banerjee, A. Pandey, U. R. Pailla, G.-S. Seo, S. Shekhar, H. Jain, Y. Lin, X. Wu, J. Bamberger, and U. Muenz, "Autonomous microgrid restoration using grid-forming inverters and smart circuit breakers," in *Proc. IEEE Power Energy Soc. Gen. Meeting (PESGM)*, Jul. 2022, pp. 1–5.

[11] R. Singh, P. Paniyil, and Z. Zhang, "Transformative role of power electronics: In solving climate emergency," *IEEE Power Electron. Mag.*, vol. 9, no. 2, pp. 39–47, Jun. 2022.

[12] X. Wang, Q. Guo, C. Tu, L. Wang, F. Xiao, and Y. Hou, "Emergency control strategy of hybrid advanced traction power supply system based on multi-device collaboration," *IEEE Trans. Transport. Electrific.*, early access, Jul. 24, 2023, doi: 10.1109/TTE.2023.3297316.

[13] G. Puleo, M. Muetherig, M. Zdrallek, and D. Aschenbrenner, "Islanding algorithm for the resupply of critical infrastructure during a prolonged blackout," in *Proc. ETG Congr.*, May 2023, pp. 1–7.

[14] F. Quinteros, D. Carrión, and M. Jaramillo, "Optimal power systems restoration based on energy quality and stability criteria," *Energies*, vol. 15, no. 6, p. 2062, Mar. 2022. [Online]. Available: https://www.mdpi.com/1996-1073/15/6/2062

[15] N. Zdolbitska, M. Delyavskyy, N. Lishchyna, V. Lishchyna, S. Lavrenchuk, and V. Sulim, "Diy smart auxiliary power supply for emergency use," in *Advances in Artificial Systems for Logistics Engineering III*, Z. Hu, Q. Zhang, and M. He, Eds. Cham, Switzerland: Springer, 2023, pp. 382–392.

[16] M. Cernan, Z. Müller, J. Tlustý, and J. Halaška, "Methodology of electricity supplying of critical infrastructure in crisis situations," in *Proc. 21st Int. Sci. Conf. Electr. Power Eng. (EPE)*, Oct. 2020, pp. 1–5.

[17] A. Subhana, F. Zahin, F. Abid, and Md. Z. R. Khan, "Emergency backup power to a rural hospital in disaster condition," in *Proc. IEEE 4th Int. Future Energy Electron. Conf. (IFEEC)*, Nov. 2019, pp. 1–5.

[18] S. Blankinship, "Georgia hospital has state-of-the-art on-site power: A state-of-the-art medical facility needed emergency backup power to match," *Power Eng.*, vol. 113, no. 11, pp. 142–144, 2009.

[19] A. Kwasinski, "Technology planning for electric power supply in critical events considering a bulk grid, backup power plants, and micro-grids," *IEEE Syst. J.*, vol. 4, no. 2, pp. 167–178, Jun. 2010.

[20] M. Ashour, "Low cost three-phase emergency power supply," in *Proc. 18th Int. Conf. Exhib. Electr. Distrib. (CIRED)*, 2005, pp. 1–6.
[21] S. Chakraborty, S. Patel, G. Saraswat, A. Maqsood, and M. V. Salapaka, "Seamless transition of critical infrastructures using droop controlled grid-forming inverters," *IEEE Trans. Ind. Electron.*, vol. 71, no. 2, pp. 1535–1546, Feb. 2024.
[22] Y. Li, L. Fu, K. Meng, Z. Y. Dong, K. Muttaqi, and W. Du, "Autonomous control strategy for microgrid operating modes smooth transition," *IEEE Access*, vol. 8, pp. 142159–142172, 2020.
[23] M. Amin and Q.-C. Zhong, "Resynchronization of distributed generation based on the universal droop controller for seamless transfer between operation modes," *IEEE Trans. Ind. Electron.*, vol. 67, no. 9, pp. 7574–7582, Sep. 2020.
[24] J. Westman, R. Hadidi, C. Fox, J. Leonard, and A. Harrell, "Controller hardware-in-the-loop testing of an IEC 61850 GOOSE based control for seamless transition of a microgrid between island and grid-connected modes," *IEEE Trans. Ind. Appl.*, vol. 57, no. 1, pp. 61–69, Jan. 2021.
[25] A. Vukojevic and S. Lukic, "Microgrid protection and control schemes for seamless transition to island and grid synchronization," *IEEE Trans. Smart Grid*, vol. 11, no. 4, pp. 2845–2855, Jul. 2020.
[26] B. Lundstrom, S. Patel, and M. V. Salapaka, "Distribution feeder-scale fast frequency response via optimal coordination of net-load resources—Part I: Solution design," *IEEE Trans. Smart Grid*, vol. 12, no. 2, pp. 1289–1302, Mar. 2021.
[27] J. Wang, S. Chakraborty, V. Khatana, B. Lundstrom, G. Sarawat, and M. Salapaka, "Evaluation of optimal net load management in microgrids using hardware-in-the-loop simulation," in *Proc. IEEE Power Energy Soc. Innov. Smart Grid Technol. Conf. (ISGT)*, Apr. 2022, pp. 1–5.
[28] J. Hu, J. Cao, J. M. Guerrero, T. Yong, and J. Yu, "Improving frequency stability based on distributed control of multiple load aggregators," *IEEE Trans. Smart Grid*, vol. 8, no. 4, pp. 1553–1567, Jul. 2017.
[29] A. M. Prostejovsky, M. Marinelli, M. Rezkalla, M. H. Syed, and E. Guillo-Sansano, "Tuningless load frequency control through active engagement of distributed resources," *IEEE Trans. Power Syst.*, vol. 33, no. 3, pp. 2929–2939, May 2018.
[30] V. Khatana, S. Chakraborty, G. Saraswat, B. Lundstorm, and M. V. Salapaka, "Evaluation of horizon of viability optimization engine for sustained power to critical infrastructure," in *Proc. IEEE Power Energy Conf. Illinois (PECI)*, Mar. 2022, pp. 1–8.
[31] C. Sun, G. Joos, and F. Bouffard, "Adaptive coordination for power and SoC limiting control of energy storage in an islanded AC microgrid with impact load," *IEEE Trans. Power Del.*, vol. 35, no. 2, pp. 580–591, Apr. 2020.
[32] L. Gan, A. Wierman, U. Topcu, N. Chen, and S. H. Low, "Real-time deferrable load control: Handling the uncertainties of renewable generation," in *Proc. 4th Int. Conf. Future energy Syst.*, May 2013, pp. 113–124.
[33] S. Haque, D. Materassi, S. Bolognani, M. Roozbehani, and M. A. Dahleh, "An efficient partial-order representation of feasible schedules for online decisions," in *Proc. IEEE 56th Annu. Conf. Decis. Control (CDC)*, Dec. 2017, pp. 2641–2646.
[34] A. Subramanian, M. J. Garcia, D. S. Callaway, K. Poolla, and P. Varaiya, "Real-time scheduling of distributed resources," *IEEE Trans. Smart Grid*, vol. 4, no. 4, pp. 2122–2130, Dec. 2013.
[35] P. Kundur, N. J. Balu, and M. G. Lauby, *Power System Stability and Control*, vol. 7. New York, NY, USA: McGraw-Hill, 1994.
[36] J. A. P. Lopes, C. L. Moreira, and A. G. Madureira, "Defining control strategies for MicroGrids islanded operation," *IEEE Trans. Power Syst.*, vol. 21, no. 2, pp. 916–924, May 2006.
[37] M. C. Chandorkar, D. M. Divan, and R. Adapa, "Control of parallel connected inverters in standalone AC supply systems," *IEEE Trans. Ind. Appl.*, vol. 29, no. 1, pp. 136–143, May 1993.
[38] *IEEE Standard for Interconnection and Interoperability of Distributed Energy Resources With Associated Electric Power Systems Interfaces—Amendment 1: To Provide More Flexibility for Adoption of Abnormal Operating Performance Category III*, IEEE Standard 1547a-2020, 2020, pp. 1–16.
[39] A. Yazdani and R. Iravani, *Voltage-Sourced Converters in Power Systems: Modeling, Control, and Applications*. Hoboken, NJ, USA: Wiley, 2010.
[40] *M Health Fairview University of Minnesota Medical Center*. Accessed: Dec. 1, 2020. [Online]. Available: https://www.fairview.org/locations/university-of-minnesota-medical-center-east-bank-hospital
[41] S. Chakraborty, J. Park, G. Saraswat, T. Meyers, J. Wang, S. Tiwari, A. Maqsood, A. Somani, and M. V. Salapaka, "Novel power-hardware-in-the-loop interface method for grid-forming inverter systems," in *Proc. 48th Annu. Conf. IEEE Ind. Electron. Soc.*, Oct. 2022, pp. 1–6.
[42] *IEEE Recommended Practice and Requirements for Harmonic Control in Electric Power Systems*, IEEE Standard 519-2014, Jun. 2014, pp. 1–29.

SOHAM CHAKRABORTY (Member, IEEE) received the B.E. degree in electrical engineering from Bengal Engineering and Science University, Shibpur, India, in 2013, and the M.Tech. degree in electrical engineering from the Indian Institute of Technology, Mumbai, in 2016. He is currently pursuing the Ph.D. degree in electrical engineering with the University of Minnesota. He was associated with the Indian Institute of Science, Bengaluru, as a Junior Research Fellow on a project funded by the Department of Science and Technology, India.

JAESANG PARK (Graduate Student Member, IEEE) received the B.S. and M.S. degrees in mechanical engineering from Yonsei University, Seoul, South Korea. He is currently pursuing the Ph.D. degree with the Department of Mechanical Science and Engineering, University of Illinois, Urbana–Champaign. He is developing a framework for renewable energy integration based on the microgrid concept, with a high bandwidth and robust physical layer augmented with an optimized economic layer. His research interests include developing robust and optimal inverter control architecture for microgrid applications.

GOVIND SARASWAT (Senior Member, IEEE) received the Bachelor of Technology degree in electrical engineering from the Indian Institute of Technology, New Delhi, India, in 2007, and the Ph.D. degree from the University of Minnesota-Twin Cities, Minneapolis, MN, USA, in 2014, with a focus on control system and dynamics. He currently works as a Researcher with the National Renewable Energy Laboratory (NREL), where his research interests include power system modeling and analysis, measurement-based operation and control, machine learning, and optimization.

TOBY MEYERS (Member, IEEE) received the B.S.E. and M.S. degrees in electrical engineering from Arizona State University, Tempe, AZ, USA, in 2018 and 2019, respectively. Since graduating, he was a Research Engineer at the National Renewable Energy Laboratory, where he developed/implemented software control algorithms for power electronics, and then joined a small inverter manufacturer, where he developed desktop software models for a utility-scale battery inverter. Currently, he is working as a Software Engineer developing high-performance financial software. His research interests include high-performance computing (HPC), numerical optimization, and secure software systems.

JING WANG (Senior Member, IEEE) received the Ph.D. degree in electrical engineering from RWTH Aachen University, Aachen, Germany, in 2015. She is currently a Senior Research Engineer with the National Renewable Energy Laboratory, Golden, CO, USA. She has expertise in power and controller hardware-in-the-loop (HIL) evaluation of microgrid controllers, advanced distribution management systems (ADMSs), distributed energy resource management systems (DERMS), DERs for grid automation and control, and DER integration studies. Her research interests include power electronics control of distributed energy resources, and microgrid modeling, protection design, and control distributed energy resources (DERs) integration.

SOUMYA TIWARI (Member, IEEE) received the B.E. degree in electronics and instrumentation engineering from the Lakshmi Narain College of Technology, Bhopal, India, in 2012, and the master's degree from San Diego State University, San Diego, CA, USA, in 2018. She was an Electrical Engineer at the Power Systems Engineering Center, National Renewable Energy Laboratory (NREL), Golden, CO, USA. Currently, she is working at Toronto Hydro as the Manager of engineering grid strategy.

VIVEK KHATANA (Graduate Student Member, IEEE) received the bachelor's degree in electrical engineering from the Indian Institute of Technology, Roorkee, in 2018. He is currently pursuing the Ph.D. degree with the Department of Electrical Engineering, University of Minnesota. His research interests include distributed optimization, distributed control, stochastic calculus, networks of dynamical systems, data-driven system identification, and data-driven control of power systems.

ATIF MAQSOOD received the B.S. degree in electrical engineering from the Lahore University of Management and Sciences, Lahore, Pakistan, in 2013, the master's degree from Clemson University, Clemson, SC, USA, in 2017, and the Ph.D. degree from the University of California at Santa Cruz, Santa Cruz, CA, USA, in 2020, with a focus on power electronics. He is an Electrical and Control Engineer at Dynapower Company, LLC, South Burlington, VT, USA. His research interests include Z-source breakers, motor drives, energy storage solutions, and digital signal processors (DSP).

APURVA SOMANI received the B.Tech. degree in electrical engineering from the Indian Institute of Technology, Kanpur, India, in 2006, and the M.S. degree in electrical engineering from the University of Minnesota, Minneapolis, in 2011, where he is currently pursuing the Ph.D. degree, researching open-end winding ac machine drives. He is currently an Electronics and Controls Engineer with Dynapower Company, LLC, South Burlington, VT, USA, where he is involved in the design and control of power electronic converters for grid-tied energy storage applications.

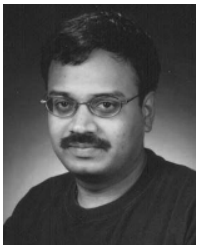

MURTI V. SALAPAKA (Fellow, IEEE) received the bachelor's degree in mechanical engineering from the Indian Institute of Technology, Madras, in 1991, and the master's and Ph.D. degrees from the University of California at Santa Barbara, Santa Barbara, 1993 and 1997, respectively. He was with the Electrical Engineering Department, Iowa State University, from 1997 to 2007. He is currently the Vincentine Hermes Luh Chair Professor with the Electrical and Computer Engineering Department, University of Minnesota, Minneapolis. He was a recipient of the NSF CAREER Award, in 1998, and the ISUYoung Engineering Faculty Research Award, in 2001.